Electronic Supplementary Information

Atomic Simulation of the Growth of Defect-free Carbon Nanotubes

Ziwei Xu,[a] TianyingYan[b*] and Feng Ding[a*]

[a]*Institute of Textiles and Clothing, Hong Kong Polytechnic University, Hong Kong, The People's Republic of China*

[b] *Institute of New Energy Material Chemistry, Collaborative Innovation Center of Chemical Science and Engineering (Tianjin), Nankai University,Tianjin 300071, The People's Republic of China*

*E-mail: feng.ding@polyu.edu.hk, tyan@nankai.edu.cn

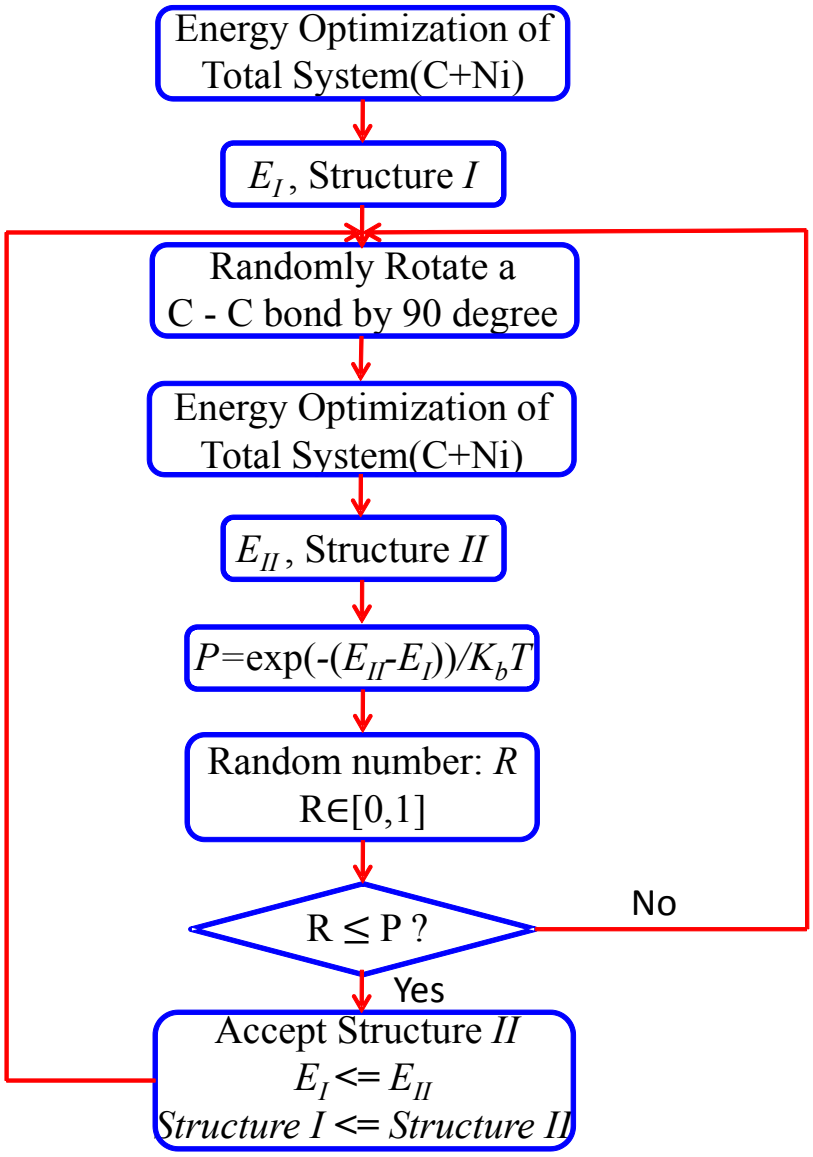

Fig. S1 Scheme of basin-hopping (BH) defects-healing strategy in the atomistic simulation.

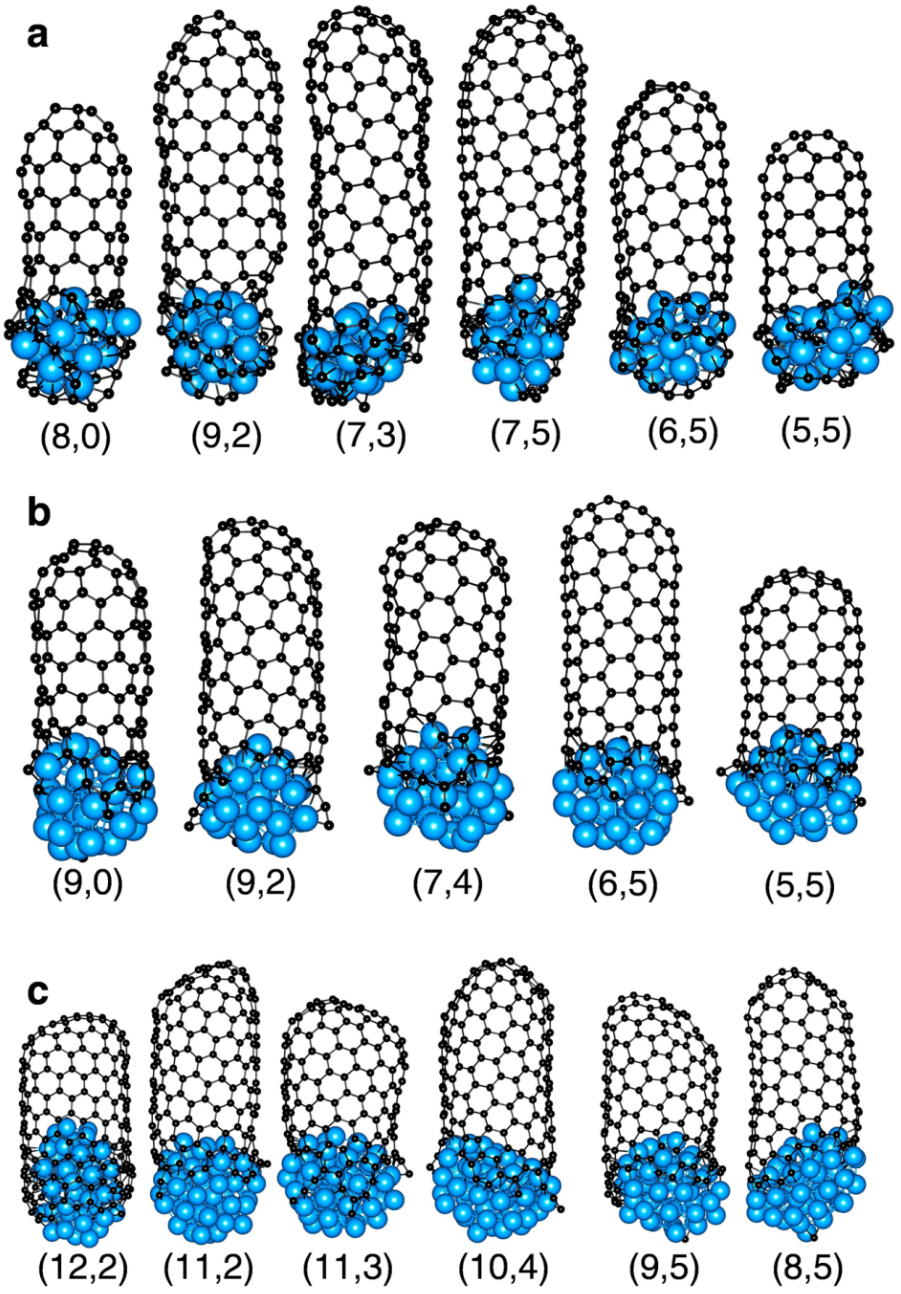

Fig. S2 Selected SWCNTs simulated by liquid catalyst particles. **(a)** Ni_{19}, **(b)** Ni_{32} and **(c)** Ni_{55}.

Development of the force field for the carbon-metal interactions

The potential energy of the whole catalytic CNT growth system can be divided into three categories, i.e.,

$$E^{tot} = E^{cc} + E^{mc} + E^{mm} \tag{S-1}$$

in which E^{cc}, E^{mc}, and E^{mm} are the carbon-carbon (C-C), metal-carbon (M-C), and metal-metal (M-M) interaction energies, respectively. Here, the metal atoms represent the catalyst particle. These three potential energy terms can be further written as,

$$E^{cc} = \sum_{i} \sum_{j(j>i)} (E_{ij}^{cc}) \tag{S-2}$$

$$E^{mc} = \sum_{i} \sum_{j} (E_{ij}^{mc}) \tag{S-3}$$

$$E^{mm} = \sum_{i} \sum_{j(j>i)} (E_{ij}^{mm}) \tag{S-4}$$

in which E_{ij}^{cc}, E_{ij}^{mc}, and E_{ij}^{mm} indicate the interaction energies of the C-C, M-C, and M-M atoms *i* and *j*, respectively.

Like the former development of the reactive empirical bond order (REBO) potential,[1] we consider the following cases for the C-C interaction: (1) a C-C bond far away from the metal particle; (2) a C-C bond on the surface of the metal particle; (3) a C-C bond under the subsurface of the metal particle; and (4) a C-C bond inside the metal particle. For the M-C interaction, in addition to the bond order from the surrounding metals, we also consider the bond order from the surrounding carbons, which determine the types of carbon atoms in the selected M-C bonds (*e.g.,* the carbon monomer, carbon dimer, carbon chain, carbon wall, AC edge or ZZ edge, *etc*.).

The important improvements of this newly developed REBO potential are mainly manifested in the M-C interaction, including the addition of (1) a parameter of local coordination to tune the M-C interaction while simplifying the form of the

original M-C potential;[1] and (2) an angle dependent term to reflect the fact that a σ bond of the C-M interaction at the edge of the carbon wall tends to be perpendicular to the metal surface.[2] It should be noted that the parameter fittings with this M-C potential are based on the density function theory (DFT) calculations of the carbon - nickel system. The details of the three interaction categories are introduced below.

S1 Carbon-Carbon interaction

The C-C interaction is mainly described by the modified REBO2 potential,[3] including the repulsive interaction term $V^R(r_{ij})$ and attractive interaction term $V^A(r_{ij})$ as functions of the distance r_{ij} between two paired atoms. A parameter α_{ij}^{cc} is added to reflect the screening effect of metal atoms on the C-C bond, which weakens the C-C interaction. As such, the C-C interaction is written as

$$E_{ij}^{cc} = \alpha_{ij}^{cc}[V^R(r_{ij}) - V^A(r_{ij})] \tag{S-5}$$

$$V^R(r_{ij}) = f^{cc}(r_{ij}) \cdot (1 + Q / r_{ij}) \cdot Ae^{-\alpha r_{ij}} \tag{S-6}$$

$$V^A(r_{ij}) = b_{ij} f^{cc}(r_{ij}) \sum_{n=1,3} (B_n e^{-\beta_n r_{ij}}) \tag{S-7}$$

in which the parameters Q, A, α, β_n, and B_n are the parameters are described in the original REBO2 potential.[3] In Eq. (S-7), b_{ij} is the bond order function, depending on the local coordination and the bond angle of carbon atoms i and j. The details of this term can also be found in the original REBO2 potential.[3] $f^{cc}(r_{ij})$ in Eq. (S6) is the switching function of the C-C repulsive interaction, i.e.,

$$f^{cc}(r_{ij}) = \begin{cases} 1, & r_{ij} < R_{cc1} \\ \left[1 + \cos\left(\pi \cdot \dfrac{r_{ij} - R_{cc1}}{R_{cc2} - R_{cc1}}\right)\right]/2, & R_{cc1} < r_{ij} < R_{cc2} \\ 0, & r_{ij} > R_{cc2} \end{cases} \tag{S-8}$$

in which R_{cc1} and R_{cc2} are two cutoff distances, as listed in table S1. In Eq. (S-5), α_{ij}^{cc} is given by

$$\alpha_{ij}^{cc} = \begin{cases} 1 & , \quad N_{ij}^{M} < N_{1}^{M} \\ \left[1 + \cos\left(\pi \cdot \dfrac{N_{ij}^{M} - N_{1}^{M}}{N_{2}^{M} - N_{1}^{M}}\right)\right]/2, & N_{1}^{M} < N_{ij}^{M} < N_{2}^{M} \\ 0 & , \quad N_{ij}^{M} > N_{2}^{M} \end{cases} \tag{S-9}$$

$$N_{ij}^{M} = (N_{i}^{M} + N_{j}^{M}) / 2 \tag{S-10}$$

in which N_{ij}^{M} is the averaged metal coordinates of atoms *i* and *j*, and thus reflects the metal environment around a C-C bond. In Eq. (S-10), N_{i}^{M} and N_{j}^{M} represent the metal coordinates of atoms *i* and *j*, respectively, as defined by equations (S-11) and (S-12) below. N_{1}^{M} and N_{2}^{M} are the cutoff numbers (see table S1). Similar to $f^{cc}(r_{ij})$ defined in equation (S-8), $f^{cm}(r_{ik})$ and $f^{cm}(r_{jk})$ in Eqs. (S-11) and (S-12) are the cutoff functions of the C-M interaction, which is defined in equation (S-13), i.e.,

$$N_{i}^{M} = \sum_{k}^{metal} f^{cm}(r_{ik}) \tag{S-11}$$

$$N_{j}^{M} = \sum_{k}^{metal} f^{cm}(r_{jk}) \tag{S-12}$$

$$f^{cm}(r_{ik}) = \begin{cases} 1 & , \quad r_{ik} < R_{cm1} \\ \left[1 + \cos\left(\pi \cdot \dfrac{r_{ik} - R_{cm1}}{R_{cm2} - R_{cm1}}\right)\right]/2, & R_{cm1} < r_{ik} < R_{cm2} \\ 0 & , \quad r_{ik} > R_{cm2} \end{cases} \tag{S-13}$$

in which R_{cm1} and R_{cm2} are the cutoff distances (see table S1). When N_{ij}^{M} exceeds N_{2}^{M}, the C-C interaction is obviously reduced to 0, which corresponds to the cases of carbon atoms dissolved into the metal particle.

Table S1 Parameters for equations (S-8), (S-9), and (S-13) with nickel as the metal catalyst.

R_{cc1} = 1.7 Å	R_{cc2} = 2.0 Å

R_{cm1} = 2.2 Å	R_{cm2} = 2.7 Å
N_1^M = 2.0	N_2^M = 6.0

S2 Metal-Carbon interaction

The M-C interaction is written as Eq. (S-14) nominally, including the distance dependence term $E_D^{mc}(r_{ij})$ and the angle dependence term $E_\theta^{mc}(r_{jk,}\, r_{jl,}\, \theta_{kjl})$, i.e.,

$$E_{ij}^{mc}(r_{ij}) = E_D^{mc}(r_{ij}) + E_\theta^{mc}(r_{jk}, r_{jl}, \theta_{ljk}) \tag{S-14}$$

Details of Eq. (S-14) are discussed below.

a) Distance dependence term $E_D^{mc}(r_{ij})$

As shown in equation (S-15), the distance dependence term also includes Morse type repulsive $V^R(r_{ij})$ and attractive $V^A(r_{ij})$ terms, in Eqs. (S-16) and (S-17), respectively.[4]

$$E_D^{mc}(r_{ij}) = \alpha_D^{mc} \cdot \left(V^R(r_{ij}) - V^A(r_{ij})\right) \tag{S-15}$$

$$V^R(r_{ij}) = f^{mc}(r_{ij})\frac{D_e}{S-1}exp\{-\beta\sqrt{2S}(r_{ij} - R_e) \tag{S-16}$$

$$V^A(r_{ij}) = f^{mc}(r_{ij})\frac{D_e S}{S-1}\exp\left\{-\beta\sqrt{\frac{2}{S}}(r_{ij} - R_e)\right\} \tag{S-17}$$

$$R_e = R_{e1} - R_{e2} \cdot exp\left(-C_R N_{ij}\right) \tag{S-18}$$

in which D_e is the equilibrium binding energy, and the parameters D_e, S, β, R_{e1}, R_{e2} and C_R are listed in table S2. In Eq. (S-18), R_e is the equilibrium distance between metal atom i and carbon atom j that depends on the coordination number N_{ij}, which indicates the environmental influence from both the surrounding metals and carbons, i.e.,

$$N_{ij} = N_j^M + \lambda N_i^C \tag{S-19}$$

$$N_j^M = \sum_{\substack{metal \\ k \neq i}} f(r_{jk}) \tag{S-20}$$

$$N_i^C = \sum_{\substack{carbon \\ l \neq j}} f(r_{il}) \tag{S-21}$$

Table S2 Parameters for the equations (S-16), (S-17) and (S-18) with the nickel as metal catalyst.

D_e = 2.6 Å	β = 1.8 Å^{-1}
R_{e1} = 1.9 Å	S = 1.3 Å
R_{e2} = 0.2 Å	C_R = 0.5

In Eq. (S-19), $\lambda = 0.08$ is the weighing parameter for the metal and carbon coordinate contributions around atoms *i* and *j*. $\alpha_D{}^{mc}$ in Eq. (S-15) is given by

$$\alpha_D^{mc} = \alpha_D^{mc}(N_j^{C1}, N_j^{C2}, N_j^M) \tag{S-22}$$

$$N_j^{C1} = \sum_{k \neq j}^{carbon} f_{jk}(r_{jk}) \tag{S-23}$$

$$N_j^{C2} = \sum_{l \neq j,k}^{carbon} f_{jl}(r_{jl}) \tag{S-24}$$

$$N_j^M = \sum_{m}^{metal} f_{jm}(r_{jm}) \tag{S-25}$$

One of the most important contributions of this newly developed M-C potential is the design of parameter α_D^{mc}, which acts as a function of (N_j^{C1}, N_j^{C2}, N_j^M), and thus can incorporate the influence of the local chemical environment surrounding the M-C bond. N_j^{C1} is the number of nearest carbon neighbors of carbon atom *j*, N_j^{C2} is the number of next nearest carbon neighbors of carbon atom *j*, and N_j^M is the number of metal coordinates around carbon atom *j*. Different compositions of (N_j^{C1}, N_j^{C2}, N_j^M) indicate different local chemical environment cases (table S3). It should be noted that

N_j^{C1}, N_j^{C2}, N_j^M are not always integers according to their definitions in equations (S-23), (S-24), and (S-25), respectively. Therefore, by fixing some of the knots of α_D^{mc}, the other α_D^{mc} values can be interpolated using the tricubic-spline interpolation. To make our potential approach as reasonable as possible, we tune these crucial knots based on the energies of some typical structures calculated by the DFT. Fig. S3 and Table S3 show the typical structures and their formation energies for the tuning of the parameter knots, respectively. Via the parameter α_D^{mc}, the effects of the local chemical environments on the M-C interaction can be taken into account. Furthermore, by tuning α_D^{mc}, we can conveniently modulate the potential for carbon-metal interactions.

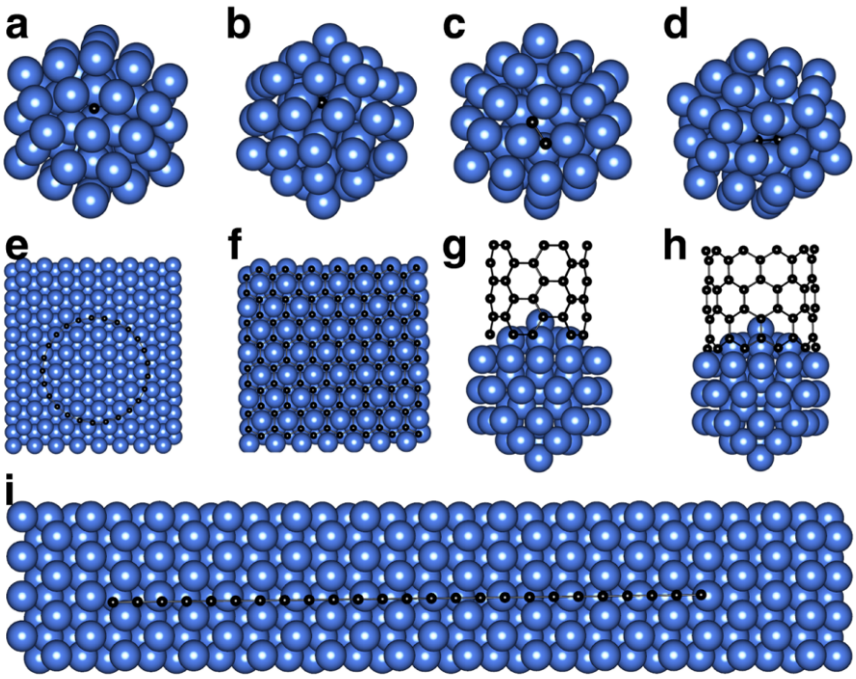

Fig. S3 Structures for adjusting the knots of α_D^{mc}. a, Carbon monomer on Ni_{55} surface. **b**, Carbon monomer in Ni_{55}. **c**, Carbon dimmer on Ni_{55} surface. **d**, Carbon dimmer in Ni_{55}. **e**, Carbon ring on Ni substrate. **f**, Carbon wall on Ni subsrate. **g**, (5, 5) carbon tube on Ni_{55}. **h**, (10, 0) carbon tube on Ni_{55}. **i**, Carbon chain with two open ends on Ni substrate.

Table S3 Formation energies E_f for different carbon-nickel systems.

Carbon Atoms	N_j^{C1}	N_j^{C2}	N_j^{M}	*E_f (eV)
#a: C monomer	0	0	1	3.7
#a: C monomer	0	0	2	2.7
#a: C monomer	0	0	3	1.2
#a: C monomer	0	0	4	0.7
#a: C monomer	0	0	5-8	0.5
#b: a C in a dimer	1	0	1	3.0
#b: a C in a dimer	1	0	2	2.0
#b: a C in a dimer	1	0	3	1.0
#b: a C in a dimer	1	0	4	0.6
#b: a C in a dimer	1	0	5-8	0.2
#c: a C in a chain	2	1,2	1,2,3,..,8	0.81
#d: a C on a Chain end	1	1	1-8	0.20
#e: a C on AC edge	2	3	1	0.30 (1.41 ev/nm)
#e: a C on AC edge	2	3	2	0.28 (1.31 ev/nm)
#e: a C on AC edge	2	3	3-8	0.268 (1.26 ev/nm)
#f: a C on a ZZ edge	2	4	1	0.20 (0.81 ev/nm)
#f: a C on a ZZ edge	2	4	2	0.18 (0.73 ev/nm)
#f: a C on a ZZ edge	2	4	3-10	0.164 (0.67 ev/nm)
#g: a C in a tube wall	3	0-6	1-8	-0.06

* $E_f = E(C_N+Ni)-E(Ni) - N*\epsilon_G$, where N is the number of carbon atoms and ϵ_G is the energy per carbon atom in the graphene. However, for e and f (C on AC and ZZ edge), the $E_f = E_{FE} - E_b$, in which E_{FE} and E_b are the formation energy of the free SWCNT end and the SWCNT-metal binding energy, respectively, and E_b is $E_b = E_{NT} + E_{Ni} - E_{NT@Ni}$, in which $E_{NT@Ni}$ is the energy of SWCNT attached on Ni_{55}, E_{NT} and E_{Ni} are energies of the isolated SWCNT and Ni_{55}, respectively. E_{FE} is defined as $E_{FE} = 0.5*(2* E_{NT2} - E_{NT1})$, in which E_{NT1} is the energy of a longer SWCNT and E_{NT2} is the energy of a shorter SWCNT, which is obtained by cutting the longer SWCNT into two equal segments. The factor 0.5 refers the fact that two open ends are formed when a SWCNT is cut into two SWCNTs.

b) Angle dependence term $E_\theta^{mc}(r_{jk,}\, r_{jl,}\, \theta_{kjl})$

The addition of the angle dependence term is another important improvement of this new potential. It was found recently that the C-M bond has a remarkable angle dependence for the carbon atoms at the edges of a graphene nanoribbon (GNR),[2] which means the σ bond tends to be perpendicular to the metal surface. To include this bond orientation preference, we add an angle dependence term in our new potential, i.e.,

$$E_{\theta}^{mc}(r_{jk}, r_{jl}, \theta_{ljk}) = \sum_{j}\left[\alpha_{ljk}\left(N_j^{C1}, N_j^{C2}\right)\cdot\left(\vec{V}_{cj}\cdot\vec{V}_{mj}\right)\right] \tag{S-26}$$

$$\vec{V}_{cj} = \sum_{l\neq j}^{carbon} f^{cc}(r_{jl})\cdot(\vec{r}_l - \vec{r}_j) \tag{S-27}$$

$$\vec{V}_{mj} = \sum_{k}^{metal} f^{cm}(r_{jk})\cdot(\vec{r}_k - \vec{r}_j) \tag{S-28}$$

$$\vec{V}_{cj}\cdot\vec{V}_{mj} = \sum_{ljk} f^{cc}(r_{jl}) f^{cm}(r_{jk}) r_{jl} r_{jk} cos\left(\theta_{ljk}\right) \tag{S-29}$$

in which θ_{ljk} is the angle between the carbon *j*-carbon *l* bond and the carbon *j*-metal *k* bond (C-C-M) (see Fig. S4). When $\theta_{ljk} = \pi$ (or $\cos\pi = -1$), the inner term of the right part of equation (S-29) obviously achieves minima. Similar to α_D^{mc}, α_{jlk} is a function of (N_j^{C1}, N_j^{C2}), which reflects the carbon coordinates around carbon *j* and determines the angle dependence magnitude for different types of carbon atoms. Just like $\alpha_{D,}^{mc}$, we fix some typical knots first and then obtain all of the α_D^{mc} values by bicubic spline interpolation. The structures used to tune the α_{jlk} knots are shown in Fig. S4 and the fixed knots are listed in table S4. By taking this angle dependence term into account, the binding energy for graphene standing on a nickel substrate where θ_{ljk} = 90° is lowered by 0.358 (eV/atom) compared with that where θ_{ljk} = 30°.

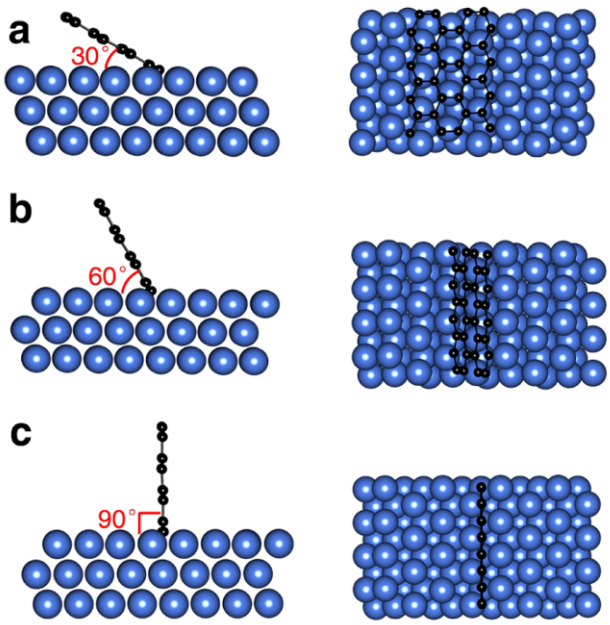

Fig. S4 Angle dependence of the C-C-M bnd. A GNR on an Ni substrate at angles of **(a)** 30º, **(b)** 60º and **(c)** 90º, respectively. The energy of **(c)** is 0.358 eV/atom lower than the one of **(a)**.

Table S4 α_{jlk} knots with nickel as the metal catalyst.

Carbon Atoms	N_j^{C1}	N_j^{C2}	α_{jlk}
C monomer	0	0	1.0
C in dimer	1	0	1.0
C in chain	2	1,2	0.01
C on a chain end	1	1,2	1.0
C on an AC edge	2	3	1.0
C on a ZZ edge	2	4	1.0
C in a tube wall	3,4,5	0-8	0.01

S3 Metal-Metal interaction

The M-M interactions of the nickel particle are descripted by the Sutton-Chen potential.[5]

$$E^{MM} = \sum_{i}^{metal} \varepsilon[\frac{1}{2}\sum_{j \neq i}^{metal} (\frac{a}{r_{ij}})^{n} - c\sqrt{\rho_i}] \quad \text{(S-30)}$$

$$\rho_i = \sum_{j \neq i}^{metal} (\frac{a}{r_{ij}})^{m} \quad \text{(S-31)}$$

where *c* is a dimensionless parameter, ε is a parameter with dimensions of energy and *a* is the lattice constant. *m* and *n* are positive integers, with *n* > *m*. The nickel particle parameters are listed in table S5.

Table S5 Parameters of Sutton-Chen potential for nickel particle.

c= 39.755	ε = 0.015731 eV	a = 3.52 Å	m = 6.0	n = 9.0

S4 Validation of the potential

Three typical carbon caps (C_{20} with a pentagon in the center and five hexagons around, C_{21} with one hexagon in the center, three pentagons and three hexagons around, C_{24} with seven pentagons in the core-shelled formation) on a Ni(111) slab surface were selected to test the accuracy of new force field (NewFF) based on the new PES. The structural characteristics, formation energies obtained by three different force fields, including the DFT, reactive force field (ReaxFF),[6, 7] Texas A&M [1] (Here, we thanks to Prof. Balbuena et al. in Texas A&M university for sharing their original code with us. For simplicity, the classical potential developed by them is named as 'Texas A&M' in our table and figures) and the newly developed force field in this study (NewFF) are shown in tables S6-S9 and Figs. S7-S8.

ReaxFF and Texas A&M are known as the best classical energy potentials that could be used to deal with chemical reactions at metal-carbon interface. Thus, we use them as the benchmarks and compare with our NewFF, which is specifically calibrated for the M-C interactions. From the following comparison, we can clearly see that:

(1) The formation energies of the three graphitic caps calculated by NewFF are

better than those calculated by ReaxFF and Texas A&M. The energetic order by Texas A&M is not consistent with the results of DFT. Although the energetic order obtained by ReaxFF is same as that calculated by DFT method, the ReaxFF underestimates formation energy by more than 60%. In comparison, NewFF not only gives same formation energy order, but in very good agreement with those calculated by DFT calculations with the largest error of ~ 20%, which is smaller than ReaxFF and Texas A&M.

(2) The optimized structures of the three caps by NewFF are similar with those optimized by ReaxFF and Texas A&M, but the results obtained by NewFF agree well with those obtained by the DFT method better than the former two.

Thus, from above discussion, we can conclude that the quality of NewFF is very high for M-C interactions, and thus the results obtained by the MD based on the newly developed potential energy surface should be more realistic.

Table S6 Comparison of formation energies* for Cap_{20}, Cap_{21} and Cap_{24} obtained by DFT calculations, ReaxFF, Texas A&M and NewFF.

E_f / Method	Cap_{20} (eV)	Cap_{21} (eV)	Cap_{24} (eV)
DFT	11.42	10.5	15.15
ReaxFF	4.34	4.03	5.75
Texas A&M	14.52	22.20	13.27
NewFF	11.50	7.79	14.56

* $E_f = E(C_N+Ni)-E(Ni) - N*\varepsilon_G$. Where, N is the number of carbon atoms and ε_G is the energy per carbon atom in the graphene.

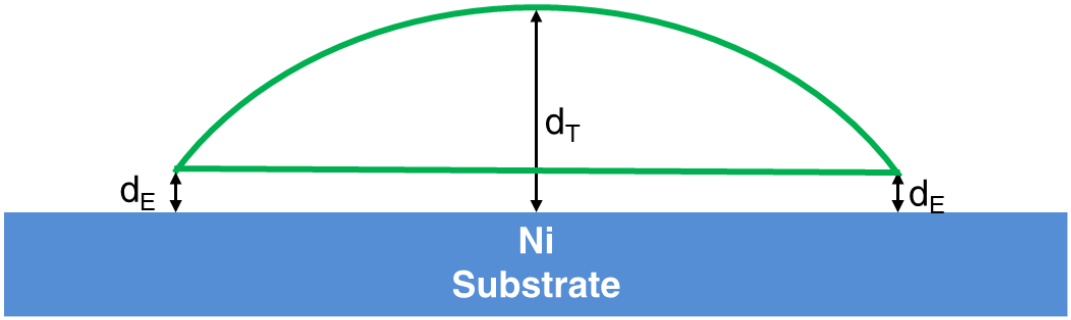

Fig. S5 The illustration of the structural characteristics, d_T and d_E, of the optimized C_{20}, C_{21} and C_{24} clusters on the Ni slab. d_T/d_E is the distances from the highest atom/edge atom to the first metal layer of the Ni(111) substrate.

Table S7 Comparison of d_T, d_E and (d_T-d_E) of Cap24.

Parameters / Force fields	d_T	d_E	(d_T-d_E)*
DFT	2.5	1.64	**1.52439**
ReaxFF	2.40	1.78	**1.348315**
Texas A&M	2.17	1.64	**1.323171**
NewFF	2.41	1.47	**1.639456**

* (d_T-d_E) is defined to compare the bending degeree of the Cap24.

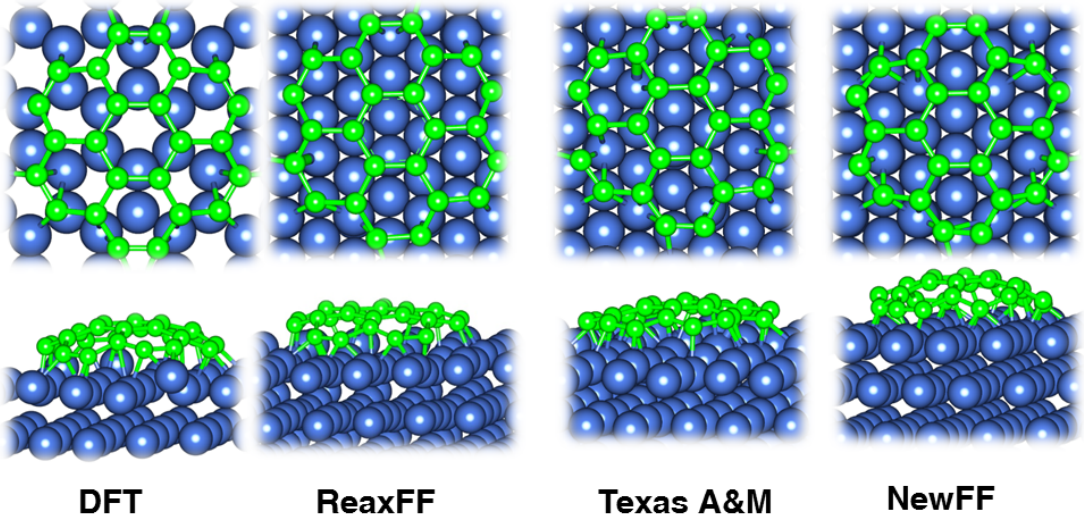

Fig. S6 Optimized configurations of C_{24} on Ni(111) slab by different force fields.

Table S8 Comparison of d_T and d_E of Cap20.

Parmeters / Force fields	d_T	d_E
DFT	2.77	1.55
ReaxFF	2.53	1.46
Texas A&M	2.41	1.57
New PES	2.73	1.40

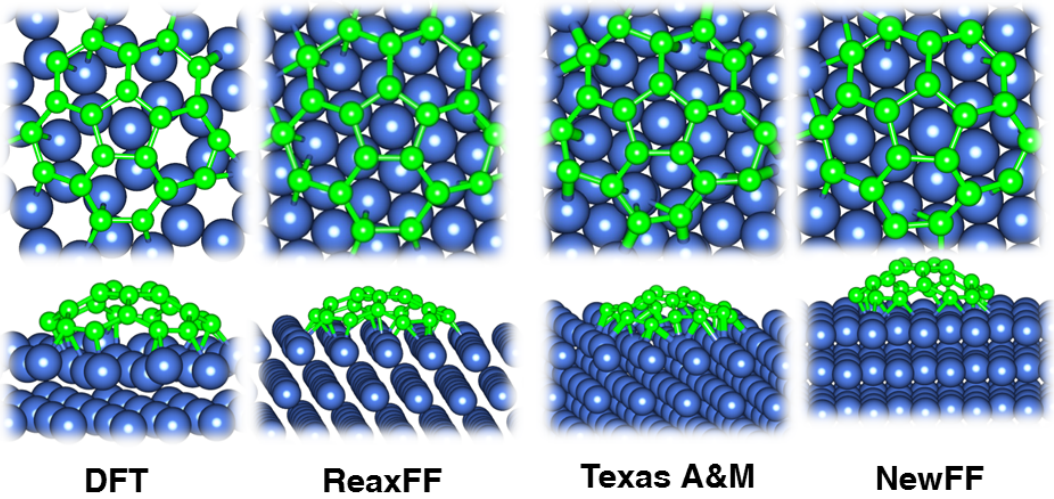

Fig. S7 The optimized configurations of C_{20} on Ni(111) surface by different force fields.

Table S9 Comparison of d_T and d_E of Cap21.

Parameter / Force fields	d_T	d_E
DFT	2.93	1.55
ReaxFF	2.68	1.34
Texas A&M	2.66	1.36
New PES	2.88	1.34

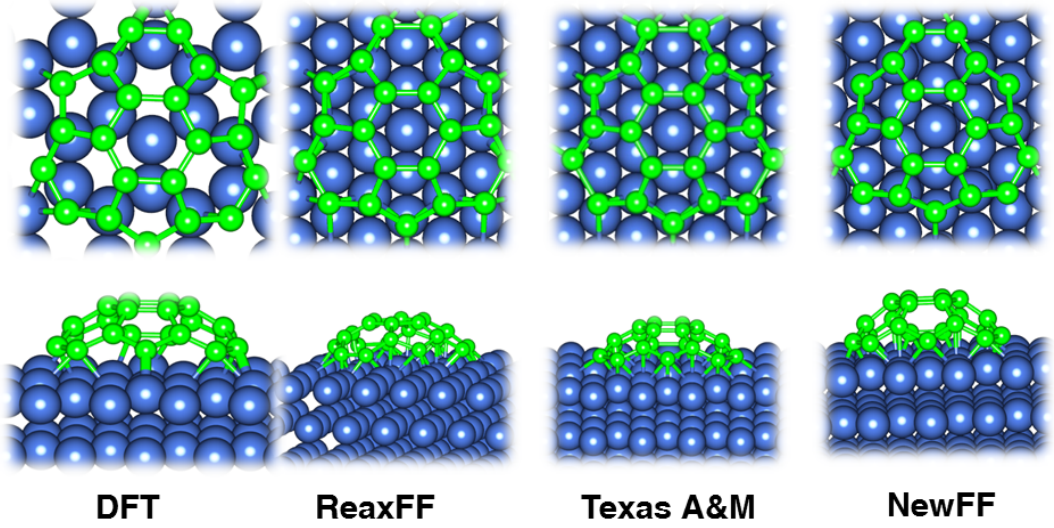

Fig. S8 Optimized configurations of C_{21} on Ni(111) surface by different force fields.

Details of density functional theory (DFT) calculation

Most of the DFT data sets used for the fitting are obtained from the previous works[8, 9] and their relative supporting information. DFT calculations are performed with the Vienna Ab-initio Simulation Package (VASP)[10, 11] The generalized gradient approximation (GGA) is adopted for the exchange correlation by using Perdew-Burke-Ernzerhof (PBE) functional, with the spin polarization taken into account.[12] The plan wave cutoff energy is set to be 400 eV and the projector-augmented wave (PAW) is used as the pseudopotential.[13] The convergence criterion for energy and force is set to be 10^{-4} eV and 0.02 eV/Å, respectively.

Defect healing during the pure MD

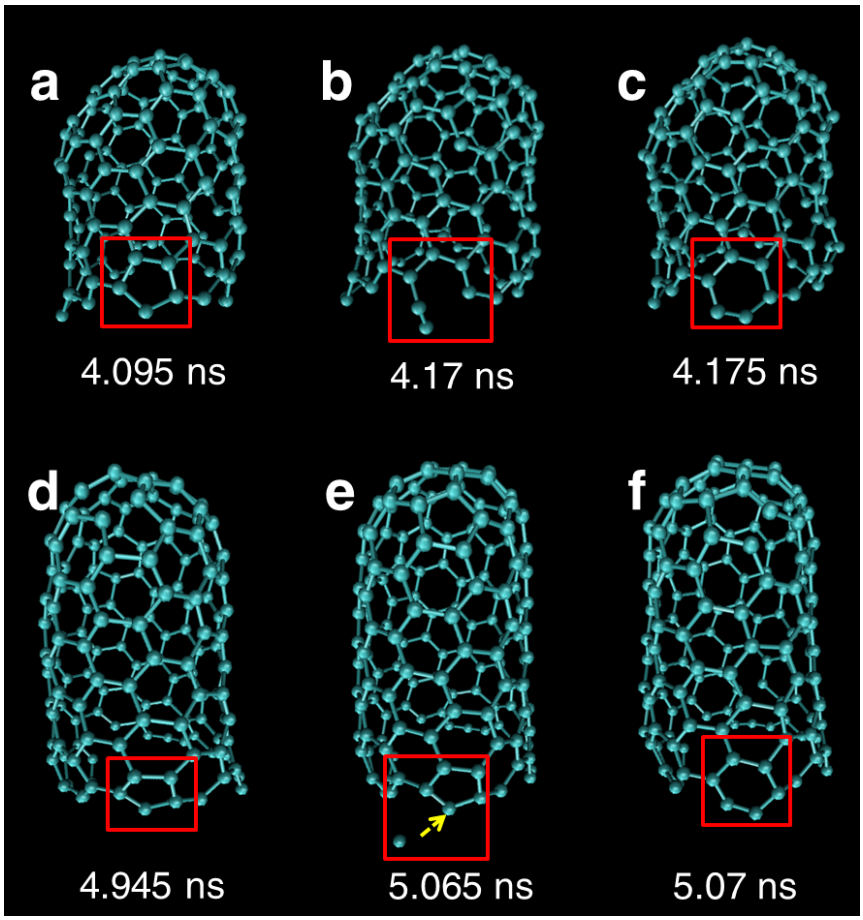

Fig. S9 (a-c) The defect of pentagon is healed to be hexagon via bond breakage and reconnection of the dangling carbon atom attached to the pentagon. (d-f) The defect of pentagon is healed to be hexagon via direct insertion of the diffused carbon atom. The catalyst is removed for sake of clear display.

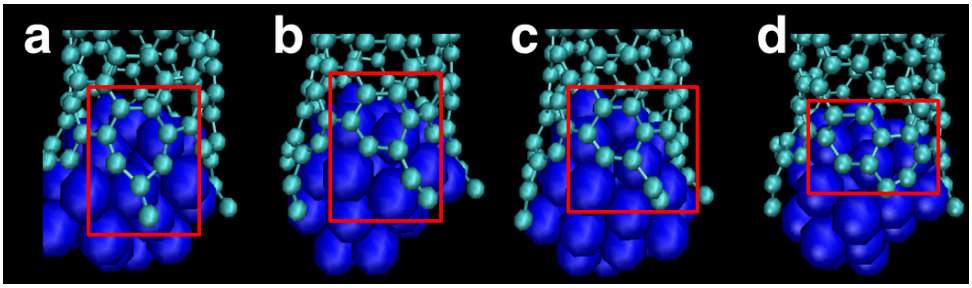

Fig. S10 (a-c) The defect of heptagon is healed by reconstruction and connection of the attached carbon atom and chains.

References:

1 A. Martinez-Limia, J. Zhao and P. B. Balbuena, *J. Mol. Model.*, 2007, **13**, 595-600.

2 Q. Yuan, H. Hu, J. Gao, F. Ding, Z. Liu and B. I. Yakobson, *J. Am. Chem. Soc.*, 2011, **133**, 16072-16079.

3 D. W. Brenner, O. A. Shenderova, J. A. Harrison, S. J. Stuart, B. Ni and S. B. Sinnott, *J. Phys.: Condens. Matter*, 2002, **14**, 783-802.

4 Y. Yamaguchi and S. Maruyama, *Eur. Phys. J. D*, 1999, **9**, 385-388.

5 A. P. Sutton and J. Chen, *Philos. Mag. Lett.*, 1990, **61**, 139-146.

6 A. C. T. van Duin, S. Dasgupta, F. Lorant and W. A. Goddard, *J. Phys. Chem. A*, 2001, **105**, 9396-9409.

7 J. E. Mueller, A. C. T. van Duin and W. A. Goddard, *J. Phys. Chem. C*, 2010, **114**, 4939-4949.

8 J. Gao, J. Yip, J. Zhao, B. I. Yakobson and F. Ding, *J. Am. Chem. Soc.*, 2012, **133**, 5009-5015.

9 Q. Yuan, J. Gao, H. Shu, J. Zhao, X. Chen and F. Ding, *J. Am. Chem. Soc.*, 2012, **134**, 2970-2975.

10 P. E. Blöchl, *Phys. Rev. B*, 1994, **50**, 17953-17979.

11 G. Kresse and J. Furthmüller, *Phys. Rev. B*, 1996, **54**, 11169-11186.

12 J. P. Perdew, K. Burke and M. Ernzerhof, *Phys. Rev. Lett.*, 1996, **77**, 3865-3868.

13 G. Kresse and D. Joubert, *Phys. Rev. B*, 1999, **59**, 1758-1775.